Joule

CellPress

Article

Poly(Ionic Liquid)s-in-Salt Electrolytes with Co-coordination-Assisted Lithium-Ion Transport for Safe Batteries

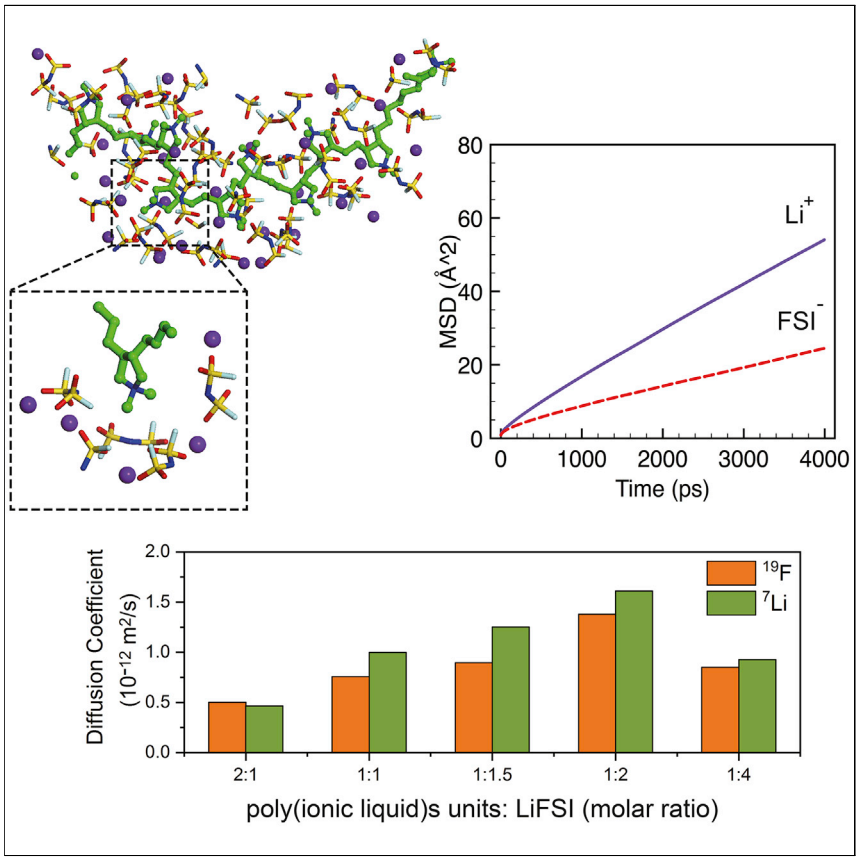

The properties of polymer hosts and their interactions with lithium salt are critically important for the design of alternative polymer electrolytes for safe lithium battery applications. Herein, we report a poly(ionic liquid) host as a solid electrolyte platform and propose a different coordination mechanism manipulating lithium-ion diffusion compared with traditional polymer systems. Our finding provides a new strategy to develop high-performance polymer electrolytes for next-generation high-energy-density lithium-metal batteries.

Xiaoen Wang, Fangfang Chen, Gaetan M.A. Girard, ..., Michel Armand, Patrick C. Howlett, Maria Forsyth

maria.forsyth@deakin.edu.au

HIGHLIGHTS

A solvent-free poly(ionic liquid)s-in-salt electrolyte is demonstrated

A co-coordination-assisted Li^+ transport is proposed for enhanced transference number

Lithium-metal batteries with high cathode loadings are demonstrated at 80°C

Wang et al., Joule 3, 2687–2702
November 20, 2019
https://doi.org/10.1016/j.joule.2019.07.008

Joule

CellPress

Article

Poly(Ionic Liquid)s-in-Salt Electrolytes with Co-coordination-Assisted Lithium-Ion Transport for Safe Batteries

Xiaoen Wang,[1,6] Fangfang Chen,[1,3,6] Gaetan M.A. Girard,[1] Haijin Zhu,[1,3] Douglas R. MacFarlane,[2] David Mecerreyes,[4] Michel Armand,[1,5] Patrick C. Howlett,[1,3] and Maria Forsyth[1,3,4,7,*]

SUMMARY

Polymer electrolytes are seen as key components for safe, high-energy-density all-solid-state lithium (Li) batteries, given their appropriate mechanical properties along with the absence of volatile and flammable solvents. Here, we report a class of solvent-free polymer electrolytes by using poly(diallyldimethylammonium) bis(fluorosulfonyl)imide (PDADMA FSI) and a high content of Li bis(fluorosulfonyl)imide (LiFSI) salt. A homogeneous mixture, with a Li^+ ion transference number of 0.56, is found at a 1:1.5 mole ratio of PDADMA FSI:LiFSI, whereas crystalline phases are observed at higher LiFSI contents. Molecular dynamics (MD) simulations indicate a co-coordination of the FSI anion with both the Li^+ and the polymer backbone, and this co-coordination is maximized at 1:1.5 mole ratio, which facilitates Li^+ transport. The optimized electrolyte has been demonstrated to support long-term stable Li-metal symmetrical cycling as well as Li-metal battery cycling (Li | $LiFePO_4$ and Li | $Li_{1/3}Ni_{1/3}Mn_{1/3}CoO_2$) at elevated temperature, with areal capacity higher than 1.1 mAh cm^{-2}.

INTRODUCTION

Lithium (Li) batteries are widespread in commercial portable electronic devices, but their extension into electric vehicles (EVs) and aerial transportation modes such as drones requires very significant improvements in their safety as well as energy density.[1] This is a major challenge for the current battery systems, which contain volatile and flammable liquid carbonate electrolytes. Although these liquid electrolytes have high ionic conductivity, their high flammability, low thermal stability, and inability to inhibit Li dendrite growth are a concern with respect to fire and explosion hazards of batteries.[2] Additionally, the conventional liquid electrolytes show a relatively narrow electrochemical stability window (ESW), which also hinders their applications with high-voltage electrode materials.[3–5] Overall, it seems that electrolyte deficiencies have become a significant barrier to further development of Li technology.

Solid polymer electrolytes are considered as promising safer alternatives to liquid electrolytes in the development of future batteries because of their good mechanical integrity and flexibility.[6,7] Unfortunately, due to inherent low ionic conductivity, most of the polymer electrolytes need to be plasticized by liquid solvent, which not only decreases the mechanical properties but also leads to similar safety concerns as for the current electrolytes.[8–10] Therefore, designing a solid polymer electrolyte system with good ion transport and robust mechanical properties and without a liquid component is a major challenge.

Context & Scale

A new solid electrolyte platform comprising a liquid-free polymerized ionic liquid (polyIL)-in-salt electrolyte is developed for application in safe lithium-metal batteries. Different from the well-known polyethylene oxide (PEO)-based electrolytes, anion-assisted co-coordination supports enhanced Li^+ transference numbers, up to 0.56. As a proof of concept, the polyIL-in-salt with optimal composition shows promising full-cell cycling performance at elevated temperature, especially when high loading of $Li_{1/3}Ni_{1/3}Mn_{1/3}CoO_2$ is used. The proposed system provides a new strategy for the development of highly efficient, solvent-free, solid polymer electrolytes with improved safety characteristics.

The first reported solid polymer electrolyte was in the 1970s when P.V. Wright discovered ionic conduction in the alkali metal-polyethylene oxide (PEO) complex, and M. Armand later demonstrated the applications of the PEO-Li salt complex as a solid-state electrolyte for Li batteries.[11,12] Since then, PEO polymers and their derivatives have been intensively investigated in both Li and sodium (Na) batteries.[13–15] Ionic conduction in PEO-salt complexes was attributed to the ether oxygen-Li^+ coordination,[16,17] when mixed with the Li salt, the ether oxygen on the PEO backbone coordinates with the Li^+, resulting in the dissociation of the Li salt and generation of mobile charge carriers.[18] Nevertheless, the Li^+ movements are limited by the "trapping" effects of the strong coordination between Li^+ and ether oxygen, which leads to relatively low conductivity and Li^+ transference number t_{Li+} (normally between 0.2 and 0.3).[19–21] Even though there have been many attempts to improve the Li^+ transport, the low Li^+ transference number is still a barrier to improving battery performance with PEO-based polymer electrolytes.

Increasing the Li salt concentration in an electrolyte has been shown to be an effective method to enhance the Li^+ transference number in some liquid-state systems.[22–24] For example, the super-concentrated alkali metal ion-based ionic liquid (IL) electrolytes support more rapid charge-discharge battery cycling than their lower metal ion concentration counterparts.[22] For polymer electrolyte systems, increasing Li salt content also has a significant effect on both ionic conductivity and Li^+ transference number. Angell et al. first proposed the concept of polymer-in-salt electrolytes, demonstrating that the glass transition temperature (T_g) of highly concentrated polymer electrolytes can be maintained below room temperature, producing a rubbery, conductive solid with relatively high electrochemical stability.[25] In another report, a polyacrylonitrile (PAN)-Li triflate ($LiSO_3CF_3$) system was observed to have fast ion transport when the salt content was above 50 wt %.[26] In this case, the authors suggested that ion transport was decoupled from T_g via morphology-related percolation effects.

With ever-increasing attempts to improve the performance of polymer electrolytes, some alternative polymer hosts such as polycarbonates (PECs),[27] polyesters,[28] polynitriles,[29] and polyalcohol were also investigated.[30] For instance, Kento et al. reported the PEC-LiFSI electrolyte with 80 wt % of LiFSI salt, showing an ionic conductivity of 10^{-5} S cm^{-1} at 30°C and a high Li transference number ($t_{Li+} > 0.5$), as well as promising battery cycling performance.[31] Interestingly, in a PEC electrolyte system containing Li bis(trifluoromethane sulfonyl)imide (LiTFSI), Brandell et al. showed that the blending of poly(trimethylene carbonate) (PTMC) at optimized ratio can increase the conductivity as high as 10^{-6} S cm^{-1} at 50°C, indicating that host polymers can affect the ion transport and conductivity.[32,33] To overcome the strong EO–Li^+ interactions, Bao et al. designed a loosely coordinated poly(tetrahydrofuran) (PTHF) host that is similar to PEO but contains fewer oxygen heteroatoms in polymer backbone.[34] Due to the weakened O-Li^+ interactions, the crosslinked PTHF-based electrolyte shows promising conductivity of 2.9×10^{-6} S cm^{-1} and a Li transference number of 0.53. Although different polymer hosts have been investigated and promising conductivity achieved, these present systems are mostly based on direct interaction between polymer backbone and Li^+, which limits the further improvement of Li^+ transport.

Poly(ionic liquid)s or polymerized ionic liquids (polyILs) have seen increasing interest as the polymer component in polymer gels or iongels, where an organic solvent or ionic liquid electrolyte, respectively, is incorporated into the polyILs.[35–37] These

[1]Institute for Frontier Materials, Deakin University, Geelong, VIC 3217, Australia

[2]School of Chemistry, Monash University, Clayton, VIC 3800, Australia

[3]ARC Centre of Excellence for Electromaterials Science (ACES), Deakin University, Burwood, VIC 3125, Australia

[4]POLYMAT University of the Basque Country UPV/EHU, Joxe Mari Korta Center, Avda. Tolosa72, 20018 Donostia-San Sebastian, Spain

[5]CIC Energigune, Parque Tecnológico de Álava, Albert Einstein 48, 01510 Miñano, Álava, Spain

[6]These authors contributed equally

[7]Lead Contact

*Correspondence: maria.forsyth@deakin.edu.au

https://doi.org/10.1016/j.joule.2019.07.008

gels typically consist of relatively low salt content, which leads to a low transference number, although they have been successfully demonstrated as polymer electrolytes for energy storage and conversion devices.[38–40] PolyIL polymers are selected due to their suitable dielectric constant for Li salt dissociation,[41] good chemical compatibility, and outstanding electrochemical stability. To date, although the ion conduction and/or transport behaviors of some pure polyIL systems have been reported,[42,43] the role of the polyIL itself on the ion dynamics of solid electrolytes has not been fully considered. In this work, we report solid-state and solvent-free polyIL-in-salt systems based on the polydiallyldimethylammonium bis(fluorosulfonyl)imide (PDADMA FSI), which can address safety issues (e.g., prevention of Li dendrite growth and non-flammability). An ionic conductivity of 0.7×10^{-4} S cm^{-1} is achieved at 80°C at a high salt concentration of 60 mol %. We investigate the effect of composition on the phase behavior, ion transport, and electrochemical performance. Computational investigations provide a molecular insight into microstructure changes, ion-ion coordination, and their impacts on ion dynamics. Based on these findings, an anion co-coordination framework is highlighted to help understand the excellent transport properties of this material. Long-term stability toward a Li-metal electrode and favorable Li-metal battery performance at elevated temperatures is demonstrated. Thus, we believe the concept of using a polyIL as a solid-state host for high concentrations of alkali metal salt for Li-metal batteries represents a promising approach toward safe and high-energy-density Li-metal batteries.

RESULTS AND DISCUSSION

Microstructure, Phase Behavior, and Ion Conductivity

Figure 1 summarizes the effect of Li salt content on electrolyte microstructure, phase behavior, and ion conductivity. The FSI-based salts were chosen for this work due to their unique properties,[22,44–46] including high Li salt solubility and enhanced alkali ion transport, as well as allowing low T_g polymers to be prepared. The mole ratio between polyIL repeat unit and LiFSI investigated in this work includes 2:1, 1:1, 1:1.5, 1:2, 1:4, and 1:6. All samples are completely dried before measurements to avoid any solvent effects (see Supplemental Experimental Procedures; Figure S1). The microstructural changes in the electrolytes can be obviously distinguished (the presence of PVDF fibers is confirmed; see Figures S2 and S3). The smooth surfaces in (b) and (c) highlight the good miscibility of the polyIL host and the LiFSI salt. With increasing Li salt content, a heterogeneous microstructure is observed, especially in 1:4 and 1:6 systems, indicating the formation of distinct phases. This is also observed from the DSC data in Figure 1G. It is known from our previous study that the pure PDADMA FSI is a rigid polymer with a T_g near 120°C,[47] suggesting that the slow segmental movements of polymer chains are due to strong ionic interactions between the small FSI anion and the charged backbone. The incorporation of Li salt into this polyIL continuously depresses the T_g to a temperature much lower than room temperature, which is distinctly in contrast with the PEO-Li salt systems.[48] For instance, in Figure 1G, the 2:1 polyIL/salt system shows only one glass transition at around 10°C, implying that the mixture is a stable and homogeneous rubber at room temperature. This significant drop in T_g in the 2:1 system compared to the pure polyIL must result from a disruption or change of the ionic interactions between the backbone and the anion in the presence of Li^+ ions. The decrease in T_g is further enhanced via the addition of more LiFSI as in 1:1, 1:1.5, and 1:2 systems. We also observe an effect of thermal history on the microstructure and phase behavior of these materials from the DSC scans on the 1:2 system after different storage times (inset in Figure 1G). During the first DSC heating cycle, additional peaks are observed above the T_g due to the formation of an intermediate phase (i.e., not

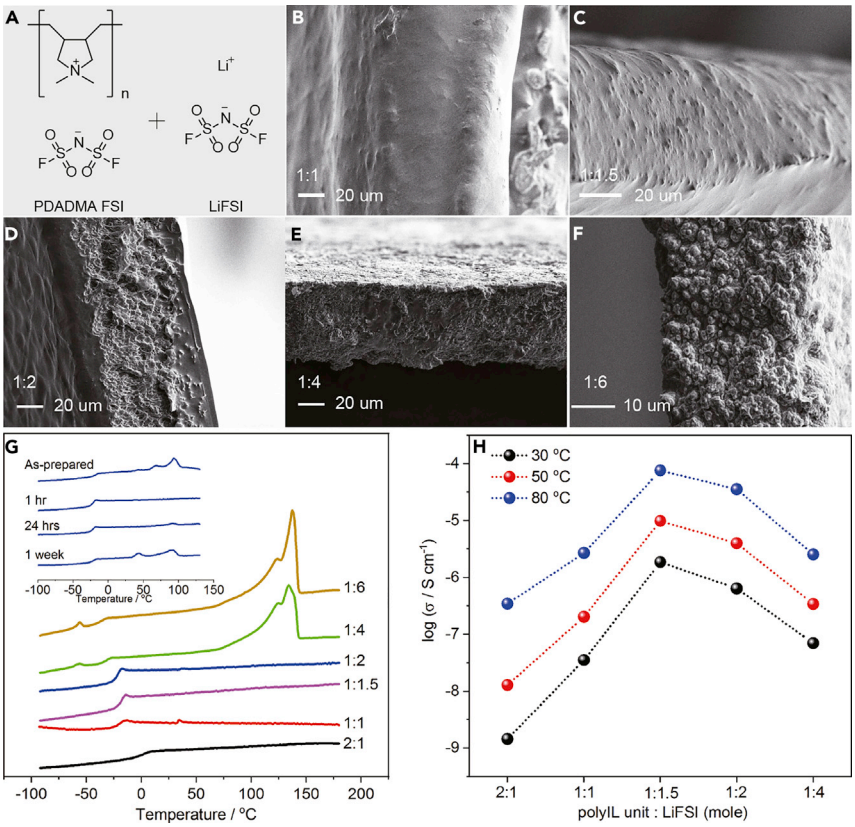

Figure 1. Li Salt Effects on Electrolyte Microstructure, Phase Behavior, and Ion Conductivity

(A) The chemical structures of poly(diallyldimethylammonium) bis(fluorosulfonyl)imide (PDADMA FSI) and Li bis(fluorosulfonyl)imide (LiFSI) salt.

(B–F) The cross-section SEM images of composite solid polymer electrolytes with different lithium salt contents. The mole ratios between polyIL repeat unit and LiFSI are (B) 1:1, (C) 1:1.5, (D) 1:2, (E) 1:4, and (F) 1:6.

(G) DSC measurement of different polyIL/salt systems shows the Li salt content effect on phase behavior of composites. The inset shows the DSC traces of the 1:2 electrolyte system with varied thermal history.

(H) The ion conductivities of different polyIL/salt systems at 30°C, 50°C, and 80°C, respectively. The highest conductivity of 0.7 × 10^{-4} S cm^{-1} is achieved for the 1:1.5 system at 80°C.

the pure LiFSI but likely a complex between the salt and the polyIL to be discussed later). These peaks disappeared during the second heating, as seen in Figure 1G, while at the same time the glass transition is more obvious and significant. Another small peak that appears near 90°C after 24 h becomes more pronounced after 1 week and is accompanied by the second peak near 50°C, which we attribute to the formation of intermediate phases. It is worth mentioning that in contrast with the 1:2 system, the DSC curve of the 1:1.5 electrolyte does not change significantly with time. For those electrolytes with higher Li salt contents (1:4 and 1:6), additional peaks appearing at −50°C (small) and 130°C (broad) are assigned to the solid-solid phase transition and final liquidus melting transition of the LiFSI salt (Figure S6), which indicates excess LiFSI is not dissolved, resulting in heterogeneity.

The effect of salt concentration on the ionic conductivity of these ionic polymer-in-salt polymer electrolytes was investigated, and the selected isothermal data from three temperatures of 30°C, 50°C, and 80°C as a function of composition are shown in Figure 1F (the full temperature dependent conductivity datasets can be found in

Figure S7). There is clearly a strong dependence of conductivity on salt concentration, as observed in this figure. The addition of Li salt gradually increases the ionic conductivity at first, which is different from what we normally observe in ionic liquid systems[46] but consistent with the decreasing T_g discussed above. Taking the result at 80°C as an example, the ionic conductivity steadily increases when the fraction of salt increases from 2:1 to 1:1.5; a further increase in LiFSI salt content eventually leads to a decrease in the ionic conductivity, as seen in the 1:2 and 1:4 systems, which could be due to the formation of significant non-conductive phases (Table S3). In all the compositions, the 1:1.5 electrolyte shows the highest ionic conductivity of 0.7×10^{-4} S cm^{-1} at 80°C and 1.1×10^{-5} S cm^{-1} at 50°C. Again, this is consistent with changes in the phase behavior observed from the DSC, which suggests crystalline phases form at the higher LiFSI concentrations. The factors that lead to this increase in ion dynamics and lowering of T_g require a deeper probe into interionic interactions, which we discuss below.

FTIR Analysis and Solid-State NMR Measurements

The changes of ion-ion interactions in the polymer electrolytes and the effect of salt content on these interactions can be clearly observed in the Fourier transform infrared (FTIR) spectra, as shown in Figure 2. The full wavenumber range spectra are given in Figure S8. In a specific region between 950 and 1,300 cm^{-1}, a vibrational peak at 1,109 cm^{-1} from the neat polyIL is assigned to the symmetrical stretching of the $-SO_2$ groups in the FSI anions.[49] After adding the Li salt, this peak continuously shifts to higher wavenumber, suggesting a change in the coordination environment of the $-SO_2$ that could be due to the increasing coordination of FSI anions with the Li^+. This change of FSI coordination environment is also supported by the significant Raman shifting of S–N–S stretching vibrations (774 and 747 cm^{-1} for LiFSI and 1:1 electrolyte, respectively; Figure S9). Therefore, we speculate that the introduced Li^+ will co-coordinate with the FSI anions from the polyIL, and this could help to break the strong anion-polycation interaction that leads to the high T_g in the pure polyIL and thus lower the T_g of the polyIL-in-salt system as observed in Figure 1.

The pulse-field gradient (PFG) diffusion measurements were performed to determine diffusivities of the Li^+ cations and FSI anions. The diffusion coefficients of the ^{7}Li (D_{7Li}), ^{19}F (D_{19F}), and the calculated D_{7Li} / (D_{19F} + D_{7Li}) are shown in Figure 3. It can be seen that the addition of LiFSI increases the diffusion coefficients of both Li^+ and FSI in going from the 2:1 to 1:1.5 system. This, again, is consistent with increased dynamics with increasing LiFSI within these materials as observed from T_g and conductivity. However, the magnitude of the increase in diffusion is perhaps surprising compared with the conductivity enhancements (nearly 2.5 orders of magnitude for conductivity and tripling of the Li^+ diffusion coefficient) given that T_g is only changing by 20°C. It is known that the ion conductivity is directly proportional to the ion mobility and ion concentration;[50] thus, we ascribe the significant increase in ion conductivity to the improved mobility and increased ion concentration from the 2:1 to 1:1.5 systems (no phase separation observed in these systems, Figure 1G). In the 1:2 and 1:4 systems, the formation of additional solid phases will inevitably decrease the mobile concentration, even though these ions have relatively high diffusivities, resulting in a decreased conductivity. Even more surprisingly, the D_{7Li} shifts from being slightly lower than D_{19F} in the 2:1 system to being significantly higher at the intermediate compositions (1:1, 1:1.5, and 1:2) and still above D_{19F} for the highest LiFSI concentration (1:4). This indicates an enhancement of Li^+ transport in these intermediate compositions and is promising with respect to these materials as solid electrolytes in Li devices, as will be demonstrated later. This improvement of Li^+ transport as salt concentration increases was also reported by

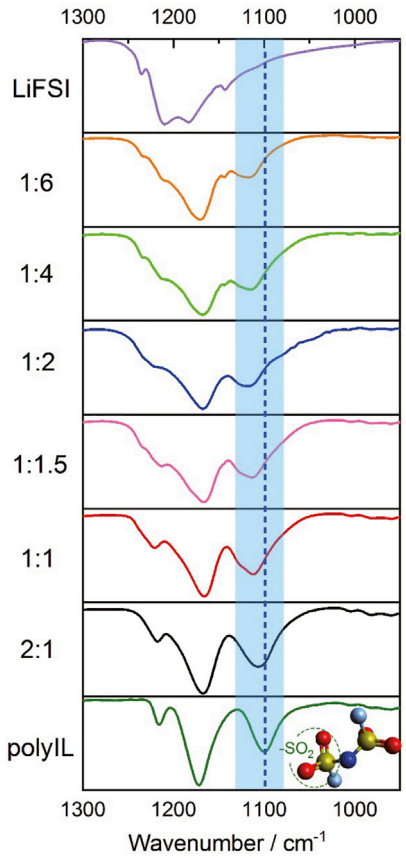

Figure 2. FTIR Spectra of PDADMA FSI (PolyIL)-LiFSI Mixtures with Different Salt Concentrations
The pure PolyIL and LiFSI were also measured for comparations. For pure PDADMA FSI, the vibrational peak located at 1,109 cm^{-1} is assigned to the symmetrical stretching of $–SO_2$ groups of the FSI anions.

Passerini et al.,[51] which is believed to be due to the change in Li^+-anion coordination environment.

Figure 3B calculates the ratio of the diffusion coefficient of Li^+ (D_{7Li}) to the sum of Li^+ and anion diffusion coefficients (D_{19F} + D_{7Li}). The ratio $D_{7Li}/(D_{19F} + D_{7Li})$ jumps from 0.48 to 0.58 when the salt content increases from 2:1 to 1:1.5, which is a good indication of the enhancement of the Li^+ transference number. On the other hand, further increasing of the Li salt content (from 1:1.5 to 1:4) leads to a significant drop of both absolute D_{7Li} and the relative diffusion (D_{7Li} is still higher than D_{19F}), which is attributed to the formation of crystalline phases and eventual crystallization of the LiFSI (Figure 1G), and thus, a decrease in the relative concentration of LiFSI actually solvated in the polyIL. Further understanding of local interactions and speciation that result in the observed behavior for the ion dynamics and resultant conductivity is provided by molecular dynamics (MD) simulations presented in the subsequent section.

MD Simulations

The changes in microstructure of polyIL upon adding LiFSI salt were investigated by MD simulations at 353 K at three polyIL repeat units to LiFSI ratios of 2:1, 1:1.5, and 1:4. A distinct change in the distribution of Li^+ is captured in Figures 4A–4C, which shows the nanoscale heterogeneous structure of the polyIL-salt systems. The 2:1 system has a polyIL dominated structure with a small fraction of the Li salt distributed in

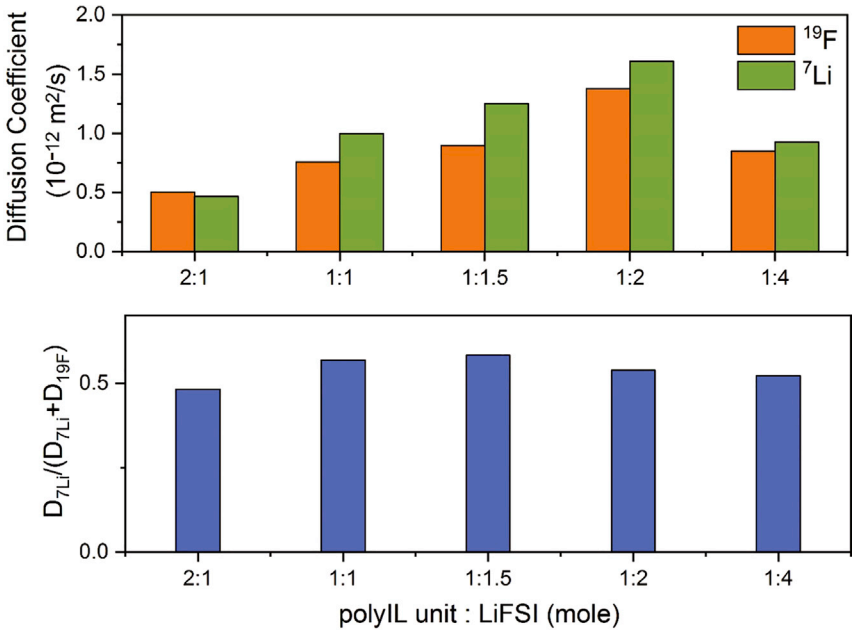

Figure 3. The Composition Dependence of the Li^+ Cations and FSI Anion Diffusivities

(A) NMR diffusion coefficient measurements of ^{19}F and ^{7}Li.

(B) The D_{7Li} / (D_{19F} + D_{7Li}) dependence on polyIL repeat unit to LiFSI mole ratio. The pulse-field gradient (PFG) diffusion measurements were performed at 80°C. At this temperature, in the higher LiFSI containing systems there are two phases, as observed from the DSC, and only the mobile phase is measured in the PFG measurement.

the polymer matrix. As the LiFSI salt content increases to 1:1.5, the Li^+ions begin to be better distributed throughout the simulation box. In the high salt concentration system (1:4), the salt-rich domains are particularly prominent, which could directly result in the crystalline phase formation, as we observed in the experiments via DSC. Unfortunately, for classic all-atom MD simulations, it is challenging to achieve the experimental equilibrated condition for 1:4 system due to limitation of simulation time and cost. The ions are trapped in an amorphous state due to their slow dynamics, and the time for ion-ion rearrangement into a crystalline phase is out of reach of current MD simulations.

Another distinct structural change happens in the nearest coordination structure of those FSI anions that are binding to the polycation. Three snapshots in Figures 4D–4F present the coordination structure of one of the single polycation chains with increasing salt concentration (2:1, 1:1.5, and 1:4). The coordinated FSI anions and Li^+ ions to this polycation chain were determined through a cutoff distance, i.e., the first minima in radial distribution functions (RDFs) between polycation and FSI, and FSI and Li^+ (Figures 4G and 4H). A significant increase in the number of Li^+ ions coordinating to FSI is demonstrated. In other words, more Li and more FSI ions are present in close proximity to the polycation chains; also, there is correspondingly more co-coordination of Li^+ and FSI pairs with the polycation, using FSI as a bridge.

A quantitative evidence to show the increased co-coordination of FSI anions with both polycations and Li ions is through their RDFs in Figures 4G–4I. Figure 4G is RDF calculated between polycation and FSI anion through their nitrogen atoms N(P) and N(F). Polycation-FSI first coordination shell is in a distance of 5.3 Å between two N atoms, and a coordination number (CN) of 1.7 is obtained. The first FSI(P)-Li^+

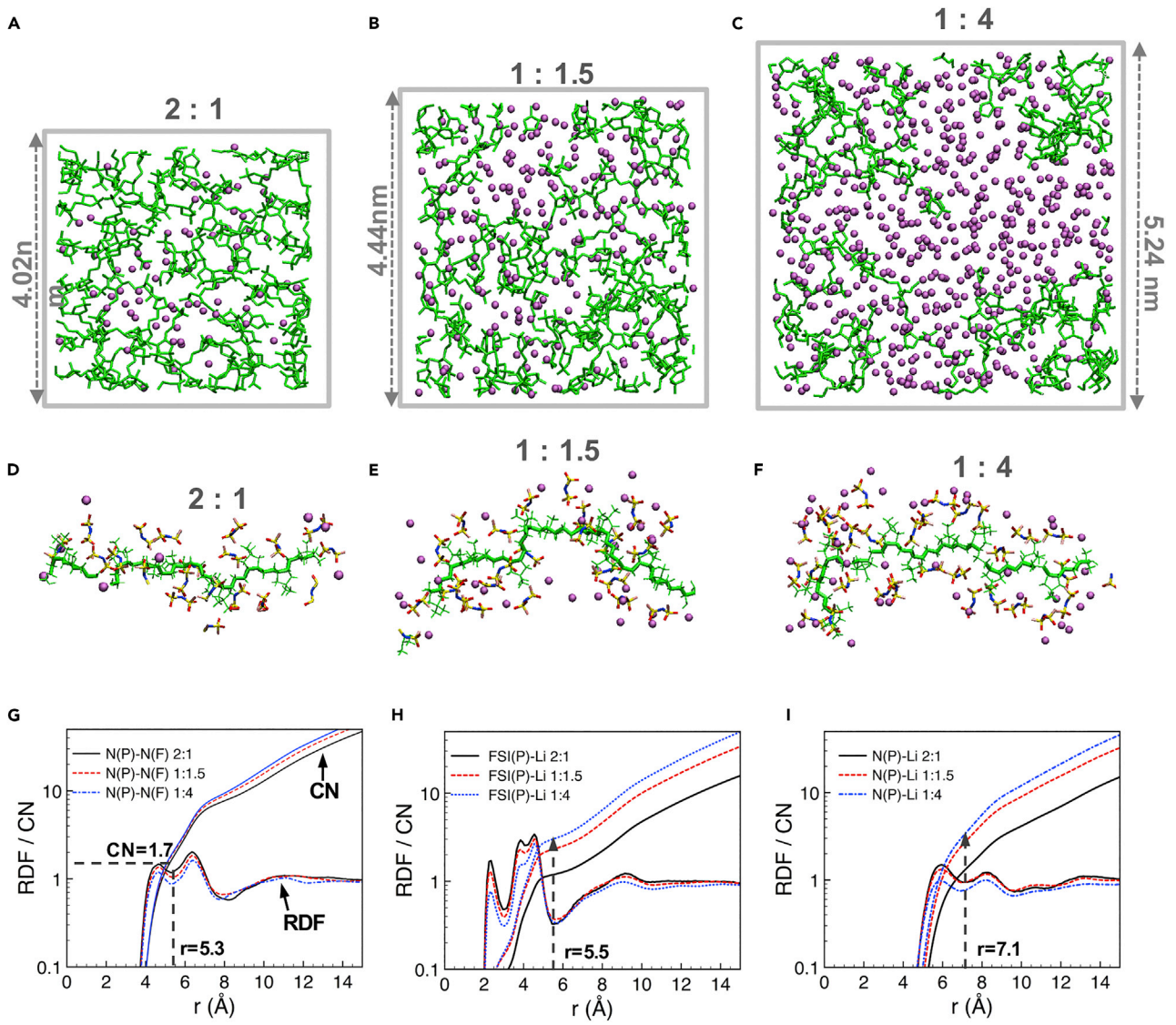

Figure 4. Electrolyte Structures with Different Li Salt Contents Demonstrated by MD Simulations

(A) Snapshot of the simulation box of the 2:1 system shows the distribution of Li^+ (purple balls represent Li^+ions) in a polymer matrix (green sticks represent polymer backbones). (B) Snapshot of the 1:1.5 system shows the presence of more Li^+ ions in the polymer matrix. (C) Snapshot of the 1:4 system shows a pronounced Li-concentrated region in the polymer matrix.

(D) A single polycation chain and its coordinating FSI anions in the 2:1 system. A small amount of Li^+ ions are also coordinated with these FSI anions. (E) A single polycation chain and its coordinated FSI anions in the 1:1.5 system. The co-coordinated Li^+ ions increase significantly. (F) In the 1:4 system, both the coordinated FSI anions and the co-coordinated Li^+ ions are further increased.(G) Radial distribution function (RDF) and coordination number (CN) calculated between nitrogen atoms from both polycation (N(P)) and FSI anion (N(F)). At the first valley position of r = 5.3 Å, CN is around 1.7 and changes less with Li concentration. (H) RDF and CN of FSI-Li^+ coordination, showing an increase in the number of Li^+ ions coordinated to the FSI anions that coordinated to polycations when Li concentration increases. (I) RDF and CN between the polycation and Li^+, which also show an increase in the number of Li^+ ions within 7.1 Å from the nitrogen atom (N(P)) in polycation at elevated Li concentrations.

FSI(P) refers to these FSI anions coordinated to polycations. The cutoff of the first coordination shell is indicated by dotted arrow lines (H, I), and the arrow shows an increase of coordination number.

coordination shell is within a distance of 5.5 Å in RDF and that of the polycation-Li^+ coordination (N(P)-Li) is within 7.1 Å in Figures 4G and 4H. This suggests the co-coordination of the FSI with both polycation and Li^+. The number of Li^+ coordinating to either polycations or FSI(P) anions (FSI(P) anions here refer to those being coordinated to polycations) shows the consistent increase at the higher salt ratios. The

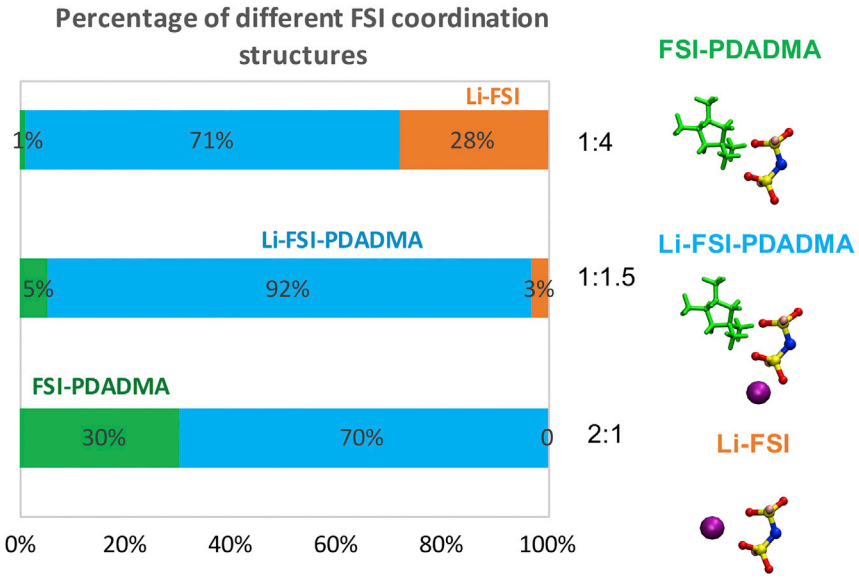

Figure 5. Percentage of Anions in Three Types of FSI Coordination Environment Calculated from MD Simulations at 353 K

The bar figures show the percentage of anions that are present in each coordination mode of FSI-PDADMA, Li-FSI-PDADMA, and Li-FSI, in each system with a different PDADMA FSI repeat unit to LiFSI ratio of 2:1, 1:1.5, and 1:4.

CN of FSI(P)-Li jumps from 1.2 in the 2:1 system to around 3 in the 1:4 system, suggesting the increased number of Li^+ that coordinates to one FSI^-. This is akin to the ion aggregation that usually occurs in ionic liquids with high concentration of Li salt. The excess salt could not participate in co-coordination with polycations and thus will tend to interact to form an energetically more favorable Li-FSI ion aggregates. This could be a pre-condition of the subsequent crystallization process observed in the experiment.

The percentage of three types of FSI anion coordination environments, including (1) FSI coordinating only the polycation (FSI-PDAD), (2) FSI coordinating only Li^+ (FSI-Li), and (3) FSI coordinating both the polycation and the Li^+ cation, was quantified and displayed in Figure 5. For the 2:1 system, 30% of the FSI anions are only coordinating to polyIL cations, while the remaining anions coordinate with both the polyIL and the Li^+ ions. For the 1:1.5 system, 92% of the FSI has a co-coordination environment that involves both polycations and Li^+ ions. This material had the highest Li^+ ionic conductivity (i.e., high overall conductivity and high D_{7Li}/D_{19F} ratio). This composition also provides the best electrochemical performance, which will be discussed later. As LiFSI concentration increases further in the 1:4 system, there is a significant increase in the Li-FSI only coordination, reaching 28% under these simulation conditions. The effect of LiFSI concentration on T_g of the polymer can also be understood here via the changes in the coordination structure of the single polymer chain.

The diffusion of ions was analyzed through calculating the mean square displacement (MSD) of Li^+ and the nitrogen atoms from both FSI and polycations at 353 K; the results are presented in Figure 6. We observe that an increase in the displacement of all types of ions occurs as LiFSI content increases, indicating that all ion movements are enhanced by the addition of the Li salt. Dynamics of Li^+ ions are also superior to the other charged ions based on the MSD results for each system,

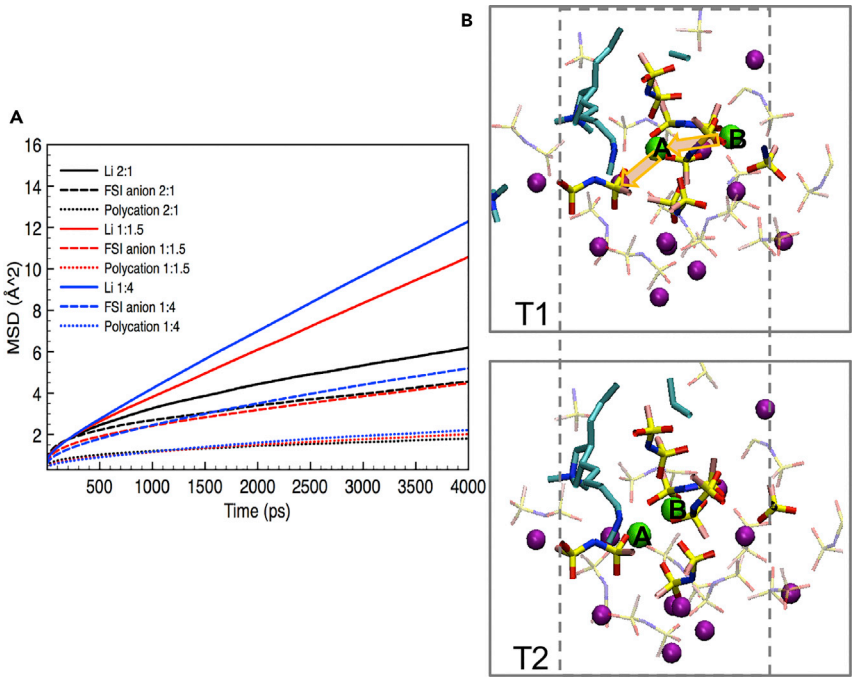

Figure 6. Mean Square Displacement of Li^+, FSI, and Polycation at 353 K and Snapshots Capturing Hopping of Two Neighboring Li^+ Ions A and B

(A) Mean square displacement (MSD) profiles indicate the relative speed of Li^+ and N atoms in both polycation and FSI when polycation repeat unit to LiFSI ratio changes between 2:1 (black lines), 1:1.5 (red lines), and 1:4 (blue lines).

(B) Snapshots taken at two time points of T1 and T2 demonstrate the correlated hopping motion of two Li^+ ions (highlighted in green color) in a connected FSI coordination environment (in the bold stick model). The rest of the Li^+ ions are in purple color. All structures presented here are within 10 Å of two hopping Li^+ ions.

which presents strong evidence of fast Li^+ motion. Furthermore, the relative motion between the Li^+ and the FSI anion from simulation is also consistent with NMR results as shown in Figure 3A. The controversial point here when comparing with experiments (e.g., conductivity and diffusion coefficients measurements) is the behavior of ion motion in the 1:4 system. In the MD simulation, this system actually shows the fastest Li^+ motion than 2:1 and 1:1.5 systems, whereas the experimental conductivity and diffusion indicate lesser dynamics. This inconsistency arises because the salt-rich region still remains amorphous in the simulated material without crystallization; therefore, a rather high motion can be maintained. Such a result is partially supported by the self-diffusion coefficients measured by NMR for the 1:2 system in Figure 3, which still remain high compared to the 1:1.5 electrolyte.

The enhanced ion dynamics upon increasing the salt content are closely related to the change in ion-ion interaction. The decrease in polymer T_g can be understood from the change in the binding strength between polycations and FSI anions. As salt content increases, more Li^+ ions start to co-coordinate to those FSI anions originally associated with the polycations only, and this reduces the interaction between polycations and FSI anions and results in more freedom in polymer backbone movement and a decreased T_g. In the case of FSI and Li^+, the formation of Li^+-FSI aggregates (or increase in the CN in the respective coordination shell of Li^+ and FSI) increases the connected Li^+-FSI coordination sites, which facilitate Li^+ hopping. Such a phenomenon is very similar to the recently reported high salt concentration

ionic liquid systems in which the Li^+ diffusion was not suppressed by the high salt concentration due to Li-anion aggregates.[45,51] The importance of the solvation-site connectivity to Li^+ transport was also emphasized by Miller et al. in polymer systems.[52] One example demonstrating this advantage is shown in Figure 6B, in which two Li^+ ions sharing connected FSI anion coordination can hop in a correlated manner, which then enhances the Li^+ diffusion. Whilst this is only qualitative at present, it does verify the importance of the exchanging coordination environment in the ion transport. A more detailed analysis of the ion dynamics to link the increased Li^+ jumping frequencies with the co-coordination environment and thus helping to further elucidate the Li^+ conduction mechanism in these materials will be undertaken in the future.

However, decreasing the glass transition does not lead to an increase in ionic conductivity, as measured experimentally, in the case of very high LiFSI content (e.g., 1:2 to 1:4). This is because in the PDADMA FSI system investigated here, the higher salt content leads to phase separation and the formation of at least one crystalline phase (as evidenced by DSC), which removes the number of "free" charge carriers. It is known than the ionic conductivity of a material is proportional to the mobility and concentration of each species.[18] Although ion dynamics increases with reduced T_g, the precipitated phases (e.g., 1:2 and 1:4 electrolytes) will significantly decrease the mobile ion concentration and increase tortuosity, which results in a lower conductivity compared with medium salt concentrations (e.g., 1:1.5 system). Thus, this simulation result points us to a possible direction for further enhancing Li^+ ion dynamics; if the richer polyIL-in-salt compositions could avoid crystallization, then increased Li^+ ion conductivities would be expected. This could possibly be achieved by tailoring the polyIL chemistry, using different anions or changing to a less crystallizable Li salt.

Electrochemistry and Battery Performance

It is shown that polyIL-LiFSI electrolytes demonstrate good thermal stability (>100°C, Figure S10) and high ESW (>5 V versus Li^+/Li, Figure S11), which enable us to investigate the electrochemistry at elevated temperatures. The Li^+ transference number (t_{Li+}) is a key parameter for developing improved electrolyte materials. A low t_{Li+} can lead to charge concentration gradients that increase cell polarization, thereby deteriorating the charge-discharge performance and long-term stability. The t_{Li+} of polyIL-in-salt polymer electrolytes were estimated by the Watanabe method,[53] and the results are shown in Figures 7A and 7B. The equivalent electric circuit (EEC) and fitted impedance spectra are shown in Figure S12. Overall, the polyIL-in-salt systems show relatively high t_{Li+} compared with the reported PEO-based system,[19] as well as recently reported electrolytes using other polymer hosts (Table S4). Particularly, the solid polymer electrolyte 1:1.5 shows a t_{Li+} of 0.56 ± 0.03 at 80°C. It is believed that the high t_{Li+} is related to the different coordination of the cationic polyILs compared with traditional PEO polymers. The movement of the FSI anions was not as "free" as in the PEO-based polymers due to non-negligible Coulombic interaction between FSI and the restricted polycations. Therefore, the high t_{Li+} is achieved due to the much higher Li^+ motion than FSI anions, a key advantage of using cationic polyIL as the polymer host in these electrolytes. In addition, the reversible oxidation and reduction behaviors in the cyclic voltammetry (CV) measurements (Figure S13) indicate that these electrolytes can sustain long-term cycling tests with reactive Li-metal electrodes. To further investigate this, we have assembled Li | Li symmetric cells and tested their cycling stability. Both polyIL-in-salt electrolytes (1:1 and 1:1.5) demonstrate stable and long-term cycling performances (up to ~100 cycles; Figure S14) at 0.1 mA cm^{-2} with low polarization, suggesting good stability and compatibility with the Li-metal

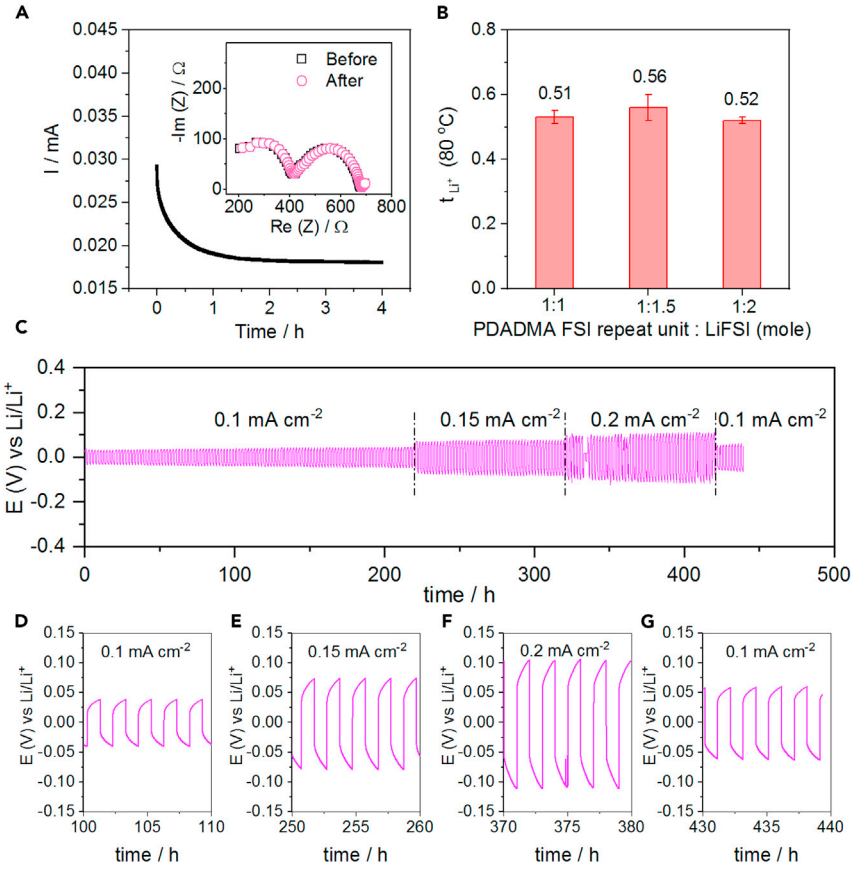

Figure 7. Li^+ Transference Numbers and Li | Li Symmetric Cell Cycling Performance

(A) Current-time curve following a DC polarization (20 mV) of the PDADMA FSI-LiFSI composite electrolyte. The polymer-to-salt ratio is 1:1.5. The inset presents the Nyquist impedance diagrams of the assembled Li | Li symmetric cell (1:1.5) before and after the polarization.

(B) The measured t_{Li+} of solid polymer electrolytes with varying polymer-to-salt ratios. The error bars are defined as the standard deviation, according to at least three individual experiments.

(C) The Li | Li symmetric cell cycling performances of polymer electrolyte 1:1 at various current densities (i.e., 0.1, 0.15, and 0.2 mA cm^{-2}).

(D–G) Selected galvanostatic cycles at each current density. (D) 0.1 mA cm^{-2}. (E) 0.15 mA cm^{-2}. (F) 0.2 mA cm^{-2} . (G) 0.1 mA cm^{-2}.The duration for each stripping or plating process is 1 h. All the measurements were completed at 80°C.

electrode. Due to the higher ionic conductivity and higher t_{Li+}, the 1:1.5 electrolytes show a lower overpotential (<50 mV at 0.1 mA cm^{-2}) during the cycling experiments compared with the 1:1 electrolyte. In addition, as shown in Figures 7C–7E, the 1:1.5 electrolyte can be further cycled at higher current densities (i.e., 0.15 and 0.2 mA cm^{-2}) without short-circuit, suggesting its capability for developing safe all solid-state batteries. The instability observed in the V-t plot (Figure 7C) after the increase to 0.2 mA/cm^2 (~330 h) may indicate an increase of active Li surface area during plating and stripping. Alternately, the pore clogging mechanism and Li surface modification,[54,55] most likely involving some significant change in the SEI, has been proposed in related IL electrolytes as another source of voltage instabilities observed in symmetric coin cells.[56]

The Li-metal full cell (Li | 1:1.5 electrolyte | $LiFePO_4$) cycling performance is demonstrated in Figures 8A and 8B. The full cell assembled with 1:1.5 electrolyte shows

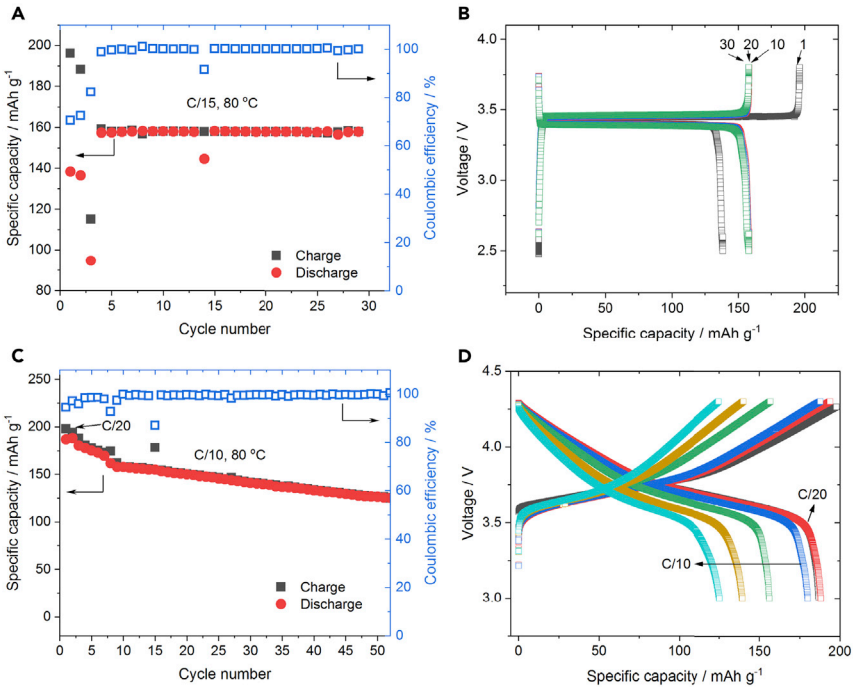

Figure 8. Charge-Discharge Performances of Li | $LiFePO_4$ Cell and Li | NMC Cell Using 1:1.5 Electrolyte

All of the measurements were conducted at 80°C.

(A and B) The cell cycling performance (A) and charge-discharge voltage curves (B) of Li | LFP cell. The cell was tested at C/15. The LFP active material loading is 3.5 mg cm^{-2}.

(C and D) The cell cycling performance (C) and charge-discharge voltage curves (D) of Li | NMC full cell. The NMC active material loading is 8.8 mg cm^{-2}. The Li | NMC cell was cycled at C/20 for the first two charge-discharge cycles, and then at C/10.

stable charge-discharge performance up to 30 cycles, even though the initial cycles display some instability. This instability could come from the activation process when a solid electrolyte is used.[57] Additionally, the low initial irreversible capacity (13%) may be due to side reactions at the cathode, which exhibits 115% of theoretical capacity in the first cycle, indicating that some of the LFP is inactive. The remainder of the irreversible capacity in the first cycle is thus expected to be mainly due to SEI formation at the Li-metal electrode. Finally, very stable cycling performance is achieved, and the discharge capacity can be maintained at 158 mAh g^{-1} (areal capacity of 1.11 mAh cm^{-2}) at C/15 with a Coulombic efficiency of 99.94% after 30 cycles.

More impressively, the 1:1.5 electrolyte can further sustain high-voltage charge-discharge cycling when assembled with high loading $Li_{1/3}Ni_{1/3}Mn_{1/3}CoO_2$ (NMC) cathode (8.8 mg cm^{-2}). As shown in Figures 8C and 8D, during the first two activation cycles at C/20, the Li | NMC cell delivers a specific capacity around 188 mAh g^{-1} (cutoff voltages of 3.0 to 4.3 V). In the following cycles at a higher charge-discharge rate of C/10 (0.12 mA cm^{-2}), although the Li | NMC cell shows some capacity degradation, a high cycling efficiency of 99.95% and a discharge capacity of 127 mAh g^{-1} (1.12 mAh cm^{-2}) are still achieved after 50 cycles. The capacity decay is likely a transition metal dissolution effect, which is accelerated at elevated temperature;[58,59] this may be improved via further optimization of the electrolyte/electrode interface for use with this cathode material. The 1:1.5 electrolyte also shows promising C-rate

performance with an initial discharge capacity above 150 mAh g^{-1} at C/5 (Figure S15). These performances also highlight the practical applications of polyIL-in-salt electrolyte in high temperature batteries, which is a strategy to greatly simplify the battery system and improve energy efficiency for EVs.[60,61] Ongoing full cell testing, including with higher voltage cathode materials, is underway to determine the full potential of these electrolytes.

Conclusion

In this study, we report the first use of a polyIL as a polymer solvent for Li salts in the absence of any liquid component and in particular with high LiFSI contents. These polyIL-in-salt systems are featured with unique co-coordination of the anion between the polymer backbone and the Li^+ ion, and this speciation appears to favor high Li diffusion and hence transference numbers of 0.56 were measured for optimum compositions at 80°C. Benefiting from the increased dynamics by adding high content Li salt, a considerable conductivity of 0.7×10^{-4} S cm^{-1} at 80°C is achieved at an optimal composition. Further FTIR and MD investigations confirm that this promising behavior arises from co-coordination effects between Li^+ and two types of FSI anions (from polyIL and LiFSI salt). The results also highlight, for the first time, the role of a polyIL, which can not only dissolve a Li salt but also participate in the transport process. The intermediate polyIL-in-salt electrolyte compositions with the optimal transport properties provide solid electrolytes with stable symmetric cycling against a Li electrode as well as promising full-cell-cycling performance. Furthermore, from the simulation data, it appears that if the chemistry of the polyIL and/or Li salt could be designed to prevent crystallization, an even higher t_{Li+} could be achieved, which provides a strategy to further improve Li^+-ion transport in polyIL-based solid electrolytes.

EXPERIMENTAL PROCEDURES

Full details of all experiments are provided in the Supplemental Information.

SUPPLEMENTAL INFORMATION

Supplemental Information can be found online at https://doi.org/10.1016/j.joule.2019.07.008.

ACKNOWLEDGMENTS

The authors would like to acknowledge the financial support of the Australia-India Strategic Research Fund, Australia (AISRF 48515). F.C., M.F., and D.R.M. would like to acknowledge the funding support from Australian Research Council (ARC) through CE140100012. The simulation work was undertaken with the assistance of resources provided at the NCI National Facility systems at the Australian National University through the National Computational Merit Allocation Scheme supported by the Australian Government. The authors would also like to thank Dr. Ruhamah Yunis for the synthesis of polymerized ionic liquids and Dr. Tiago C. Mendes for the Raman measurements and discussion. Deakin University's Advanced Characterisation Facility is acknowledged for use of the NMR facility. The authors also thank the Battery Technology Research and Innovation Hub (BatTRI-Hub) at Deakin University for their battery prototyping facilities. D.M. and M.F. also acknowledge the Basque Foundation for Science, E-48011 Bilbao, Spain.

AUTHOR CONTRIBUTIONS

X.W., D.R.M., and M.F. conceived the idea. X.W. conducted the electrolyte preparation and characterization. X.W. and G.M.A.G. carried out the electrochemistry

and battery measurements. F.C. performed MD simulations. H.Z. conducted the NMR experiments. X.W. and F.C. co-wrote the manuscript under supervision of M.F. D.M., M.A., and P.C.H. assisted with data analysis, discussion, and manuscript revision.

DECLARATION OF INTERESTS

The authors declare no competing interests.

Received: March 12, 2019
Revised: May 28, 2019
Accepted: July 9, 2019
Published: August 7, 2019

REFERENCES

1. Tarascon, J.-M., and Armand, M. (2001). Issues and challenges facing rechargeable lithium batteries. Nature *414*, 359–367.

2. Xu, K. (2004). Nonaqueous liquid electrolytes for lithium-based rechargeable batteries. Chem. Rev. *104*, 4303–4418.

3. Kanamura, K. (1999). Anodic oxidation of nonaqueous electrolytes on cathode materials and current collectors for rechargeable lithium batteries. J. Power Sources *81–82*, 123–129.

4. Moshkovich, M., Cojocaru, M., Gottlieb, H.E., and Aurbach, D. (2001). The study of the anodic stability of alkyl carbonate solutions by in situ FTIR spectroscopy, EQCM, NMR and MS. J. Electroanal. Chem. *497*, 84–96.

5. Chen, S., Wen, K., Fan, J., Bando, Y., and Golberg, D. (2018). Progress and future prospects of high-voltage and high-safety electrolytes in advanced lithium batteries: from liquid to solid electrolytes. J. Mater. Chem. A *6*, 11631–11663.

6. Di Noto, V., Lavina, S., Giffin, G.A., Negro, E., and Scrosati, B. (2011). Polymer electrolytes: present, past and future. Electrochim. Acta *57*, 4–13.

7. Mindemark, J., Lacey, M.J., Bowden, T., and Brandell, D. (2018). Beyond PEO—alternative host materials for Li+-conducting solid polymer electrolytes. Prog. Polym. Sci. *81*, 114–143.

8. Wang, X., Gong, C., He, D., Xue, Z., Chen, C., Liao, Y., and Xie, X. (2014). Gelled microporous polymer electrolyte with low liquid leakage for lithium-ion batteries. J. Membr. Sci. *454*, 298–304.

9. Qin, B., Liu, Z., Zheng, J., Hu, P., Ding, G., Zhang, C., Zhao, J., Kong, D., and Cui, G. (2015). Single-ion dominantly conducting polyborates towards high performance electrolytes in lithium batteries. J. Mater. Chem. A *3*, 7773–7779.

10. Cheng, X., Pan, J., Zhao, Y., Liao, M., and Peng, H. (2018). Gel polymer electrolytes for electrochemical energy storage. Adv. Energy Mater. *8*, 1702184.

11. Armand, M., Chabagno, J.M., and Duclot, M. (1978). Polymeric solid electrolytes. Second International Meeting on Solid Electrolytes, St. Andrews, Scotland.

12. Fenton, D.E., Parker, J.M., and Wright, P.V. (1973). Complexes of alkali metal ions with poly (ethylene oxide). Polymer *14*, 589.

13. Judez, X., Zhang, H., Li, C., González-Marcos, J.A., Zhou, Z., Armand, M., and Rodriguez-Martinez, L.M. (2017). Lithium bis(fluorosulfonyl)imide/poly(ethylene oxide) polymer electrolyte for all solid-state Li–S Cell. J. Phys. Chem. Lett. *8*, 1956–1960.

14. Xue, Z., He, D., and Xie, X. (2015). Poly(ethylene oxide)-based electrolytes for lithium-ion batteries. J. Mater. Chem. A *3*, 19218–19253.

15. Boschin, A., and Johansson, P. (2015). Characterization of NaX (X: TFSI, FSI) – PEO based solid polymer electrolytes for sodium batteries. Electrochim. Acta *175*, 124–133.

16. Johansson, P., Tegenfeldt, J., and Lindgren, J. (1999). Modelling amorphous lithium salt–PEO polymer electrolytes: ab initio calculations of lithium ion–tetra-, penta- and hexaglyme complexes. Polymer *40*, 4399–4406.

17. Molinari, N., Mailoa, J.P., and Kozinsky, B. (2018). Effect of salt concentration on ion clustering and transport in polymer solid electrolytes: a molecular dynamics study of PEO–LiTFSI. Chem. Mater. *30*, 6298–6306.

18. Ratner, M.A., and Shriver, D.F. (1988). Ion transport in solvent-free polymers. Chem. Rev. *88*, 109–124.

19. Zhang, H., Liu, C., Zheng, L., Xu, F., Feng, W., Li, H., Huang, X., Armand, M., Nie, J., and Zhou, Z. (2014). Lithium bis(fluorosulfonyl)imide/poly(ethylene oxide) polymer electrolyte. Electrochim. Acta *133*, 529–538.

20. Itoh, T., Fujita, K., Uno, T., and Kubo, M. (2017). Polymer electrolytes based on vinyl ethers with various EO chain length and their polymer electrolytes cross-linked by electron beam irradiation. Ionics *23*, 257–264.

21. Capiglia, C., Mustarelli, P., Quartarone, E., Tomasi, C., and Magistris, A. (1999). Effects of nanoscale SiO2 on the thermal and transport properties of solvent-free, poly(ethylene oxide) (PEO)-based polymer electrolytes. Solid State Ion. *118*, 73–79.

22. Yoon, H., Howlett, P.C., Best, A.S., Forsyth, M., and MacFarlane, D.R. (2013). Fast charge/discharge of Li metal batteries using an ionic liquid electrolyte. J. Electrochem. Soc. *160*, A1629–A1637.

23. Yoshida, K., Tsuchiya, M., Tachikawa, N., Dokko, K., and Watanabe, M. (2011). Change from glyme solutions to quasi-ionic liquids for binary mixtures consisting of lithium bis(trifluoromethanesulfonyl)amide and glymes. J. Phys. Chem. C *115*, 18384–18394.

24. Lundgren, H., Scheers, J., Behm, M., and Lindbergh, G. (2015). Characterization of the mass-transport phenomena in a superconcentrated LiTFSI:acetonitrile electrolyte. J. Electrochem. Soc. *162*, A1334–A1340.

25. Angell, C.A., Liu, C., and Sanchez, E. (1993). Rubbery solid electrolytes with dominant cationic transport and high ambient conductivity. Nature *362*, 137–139.

26. Forsyth, M., Sun, J., Macfarlane, D.R., and Hill, A.J. (2000). Compositional dependence of free volume in PAN/$LiCF_3SO_3$ polymer-in-salt electrolytes and the effect on ionic conductivity. J. Polym. Sci. B Polym. Phys. *38*, 341–350.

27. Sun, B., Mindemark, J., Edström, K., and Brandell, D. (2014). Polycarbonate-based solid polymer electrolytes for Li-ion batteries. Solid State Ion. *262*, 738–742.

28. Wu, I.D., and Chang, F.-C. (2007). Determination of the interaction within polyester-based solid polymer electrolyte using FTIR spectroscopy. Polymer *48*, 989–996.

29. Yoon, H.-K., Chung, W.-S., and Jo, N.-J. (2004). Study on ionic transport mechanism and interactions between salt and polymer chain in PAN based solid polymer electrolytes containing LiCF3SO3. Electrochim. Acta *50*, 289–293.

30. Kanbara, T., Inami, M., Yamamoto, T., Nishikata, A., Tsuru, T., Watanabe, M., and Ogata, N. (1989). New lithium salt ionic conductor using poly(vinyl alcohol) matrix. Chem. Lett. *18*, 1913–1916.

31. Kimura, K., Yajima, M., and Tominaga, Y. (2016). A highly-concentrated poly(ethylene carbonate)-based electrolyte for all-solid-state Li battery working at room temperature. Electrochemistry Communications *66*, 46–48.

32. Kimura, K., Motomatsu, J., and Tominaga, Y. (2016). Correlation between solvation structure and ion-conductive behavior of concentrated poly(ethylene carbonate)-based electrolytes. J. Phys. Chem. C *120*, 12385–12391.

33. Li, Z., Mogensen, R., Mindemark, J., Bowden, T., Brandell, D., and Tominaga, Y. (2018). Ion-conductive and thermal properties of a synergistic poly(ethylene carbonate)/poly(trimethylene carbonate) blend electrolyte. Macromol. Rapid Commun. *39*, 1800146.

34. Mackanic, D.G., Michaels, W., Lee, M., Feng, D., Lopez, J., Qin, J., Cui, Y., and Bao, Z. (2018). Crosslinked poly(tetrahydrofuran) as a loosely coordinating polymer electrolyte. Adv. Energy Mater. *8*, 1800703.

35. Washiro, S., Yoshizawa, M., Nakajima, H., and Ohno, H. (2004). Highly ion conductive flexible films composed of network polymers based on polymerizable ionic liquids. Polymer *45*, 1577–1582.

36. Pont, A.-L., Marcilla, R., De Meatza, I., Grande, H., and Mecerreyes, D. (2009). Pyrrolidinium-based polymeric ionic liquids as mechanically and electrochemically stable polymer electrolytes. J. Power Sources *188*, 558–563.

37. Forsyth, M., Porcarelli, L., Wang, X., Goujon, N., and Mecerreyes, D. (2019). Innovative electrolytes based on ionic liquids and polymers for next-generation solid-state batteries. Acc. Chem. Res. *52*, 686–694.

38. Li, M., Yang, L., Fang, S., Dong, S., Hirano, S.-i., and Tachibana, K. (2012). Polymerized ionic liquids with guanidinium cations as host for gel polymer electrolytes in lithium metal batteries. Polym. Int. *61*, 259–264.

39. Shaplov, A.S., Marcilla, R., and Mecerreyes, D. (2015). Recent advances in innovative polymer electrolytes based on poly(ionic liquid)s. Electrochim. Acta *175*, 18–34.

40. Wang, X., Zhu, H., Girard, G.A., Yunis, R., MacFarlane, D.R., Mecerreyes, D., Bhattacharyya, A.J., Howlett, P.C., and Forsyth, M. (2017). Preparation and characterization of gel polymer electrolytes using poly(ionic liquids) and high lithium salt concentration ionic liquids. J. Mater. Chem. A *5*, 23844–23852.

41. Tang, J., Radosz, M., and Shen, Y. (2008). Poly(ionic liquid)s as optically transparent microwave-absorbing materials. Macromolecules *41*, 493–496.

42. Mogurampelly, S., Keith, J.R., and Ganesan, V. (2017). Mechanisms underlying ion transport in polymerized ionic liquids. J. Am. Chem. Soc. *139*, 9511–9514.

43. Iacob, C., Matsumoto, A., Brennan, M., Liu, H., Paddison, S.J., Urakawa, O., Inoue, T., Sangoro, J., and Runt, J. (2017). Polymerized ionic liquids: correlation of ionic conductivity with nanoscale morphology and counterion volume. ACS Macro Lett. *6*, 941–946.

44. Forsyth, M., Girard, G.M.A., Basile, A., Hilder, M., MacFarlane, D.R., Chen, F., and Howlett, P.C. (2016). Inorganic-organic ionic liquid electrolytes enabling high energy-density metal electrodes for energy storage. Electrochim. Acta *220*, 609–617.

45. Chen, F., Howlett, P., and Forsyth, M. (2018). Na-Ion solvation and high transference number in superconcentrated ionic liquid electrolytes: a theoretical approach. J. Phys. Chem. C *122*, 105–114.

46. Girard, G.M.A., Hilder, M., Zhu, H., Nucciarone, D., Whitbread, K., Zavorine, S., Moser, M., Forsyth, M., MacFarlane, D.R., and Howlett, P.C. (2015). Electrochemical and physicochemical properties of small phosphonium cation ionic liquid electrolytes with high lithium salt content. Phys. Chem. Chem. Phys. *17*, 8706–8713.

47. Yunis, R., Girard, G.M.A., Wang, X., Zhu, H., Bhattacharyya, A.J., Howlett, P., MacFarlane, D.R., and Forsyth, M. (2018). The anion effect in ternary electrolyte systems using poly(diallyldimethylammonium) and phosphonium-based ionic liquid with high lithium salt concentration. Solid State Ion. *327*, 83–92.

48. Tominaga, Y., and Yamazaki, K. (2014). Fast Li-ion conduction in poly(ethylene carbonate)-based electrolytes and composites filled with TiO_2 nanoparticles. Chem. Commun. *50*, 4448–4450.

49. Noor, S.A.M., Su, N.C., Khoon, L.T., Mohamed, N.S., Ahmad, A., Yahya, M.Z.A., Zhu, H., Forsyth, M., and MacFarlane, D.R. (2017). Properties of high Na-ion content N-propyl-N-methylpyrrolidinium bis(Fluorosulfonyl)imide -ethylene carbonate electrolytes. Electrochim. Acta *247*, 983–993.

50. Munar, A., Andrio, A., Iserte, R., and Compañ, V. (2011). Ionic conductivity and diffusion coefficients of lithium salt polymer electrolytes measured with dielectric spectroscopy. J. Noncryst. Solids *357*, 3064–3069.

51. Giffin, G.A., Moretti, A., Jeong, S., Pilar, K., Brinkkötter, M., Greenbaum, S.G., Schönhoff, M., and Passerini, S. (2018). Connection between lithium coordination and lithium diffusion in $[Pyr_{12O1}][FTFSI]$ ionic liquid electrolytes. ChemSusChem *11*, 1981–1989.

52. Miller, T.F., Wang, Z.G., Coates, G.W., and Balsara, N.P. (2017). Designing polymer electrolytes for safe and high capacity rechargeable lithium batteries. Acc. Chem. Res. *50*, 590–593.

53. Watanabe, M., Nagano, S., Sanui, K., and Ogata, N. (1988). Estimation of Li+ transport number in polymer electrolytes by the combination of complex impedance and potentiostatic polarization measurements. Solid State Ion. *28–30*, 911–917.

54. Grande, L., von Zamory, J., Koch, S.L., Kalhoff, J., Paillard, E., and Passerini, S. (2015). Homogeneous lithium electrodeposition with pyrrolidinium-based ionic liquid electrolytes. ACS Appl. Mater. Interfaces *7*, 5950–5958.

55. Grande, L., Paillard, E., Kim, G.T., Monaco, S., and Passerini, S. (2014). Ionic liquid electrolytes for Li–air batteries: lithium metal cycling. Int. J. Mol. Sci. *15*, 8122–8137.

56. Girard, G.M.A., Hilder, M., Nucciarone, D., Whitbread, K., Zavorine, S., Moser, M., Forsyth, M., MacFarlane, D.R., and Howlett, P.C. (2017). Role of Li concentration and the SEI layer in enabling high performance Li metal electrodes using a phosphonium bis(fluorosulfonyl)imide ionic liquid. J. Phys. Chem. C *121*, 21087–21095.

57. Wang, X., Zhu, H., Greene, G.W., Zhou, Y., Yoshizawa-Fujita, M., Miyachi, Y., Armand, M., Forsyth, M., Pringle, J.M., and Howlett, P.C. (2017). Organic ionic plastic crystal-based composite electrolyte with surface enhanced ion transport and its use in all-solid-state lithium batteries. Adv. Mater. Technol. *2*, 1700046.

58. Bodenes, L., Naturel, R., Martinez, H., Dedryvère, R., Menetrier, M., Croguennec, L., Pérès, J.-P., Tessier, C., and Fischer, F. (2013). Lithium secondary batteries working at very high temperature: capacity fade and understanding of aging mechanisms. J. Power Sources *236*, 265–275.

59. Jalkanen, K., Karppinen, J., Skogström, L., Laurila, T., Nisula, M., and Vuorilehto, K. (2015). Cycle aging of commercial NMC/graphite pouch cells at different temperatures. Appl. Energy *154*, 160–172.

60. Lang, G., Kitanoski, F., and Kussmann, C. (2007). Principal aspects and simulation of a hybrid demonstrator vehicle's cooling system. SAE Tech. *1*.

61. Oltean, G., Plylahan, N., Ihrfors, C., Wei, W., Xu, C., Edström, K., Nyholm, L., Johansson, P., and Gustafsson, T. (2018). Towards Li-ion batteries operating at 80°C: ionic liquid versus conventional liquid electrolytes. Batteries *4*, 2.